14th AIAA/CEAS Aeroacoustics Conference (29th AIAA Aeroacoustics Conference)
5 - 7 May 2008, Vancouver, British Columbia Canada

AIAA 2008-2893

Interior Duct Wall Pressure Downstream of a Low-Speed Rotor

Scott C. Morris*, David B. Stephens†, Thomas D. Economon‡, William K. Blake§
University of Notre Dame, Notre Dame, Indiana, 46556 USA

The region downstream of a ducted rotor has been experimentally investigated in terms of its wake characteristics and the duct wall pressure fluctuations. The motivation for the measurements was to document and understand the sources of structural excitation that would lead to shell vibration. The wake measurements indicated a swirling hydrodynamic flow field that decayed rapidly in the streamwise direction. The interior duct wall pressure similarly indicated strong decay in the fluctuation levels in the streamwise direction. The spectral features of the wall pressure at various speeds and axial positions were described, and found to be influenced by the relative interactions of the blade rate harmonics and the duct cut-on modes. A circumferential modal analysis was used to describe the specific features of the hydrodynamic and acoustic pressure components.

I. Introduction

THE prediction of sound generated by turbomachines operating within a cylindrical duct represents one of the canonical aeroacoustic problems. A significant source of radiated sound can be structure-borne when the duct material is elastic. Direct mechanical forces as well as fluid pressure at the wall can lead to excitation of the structure. The unsteady surface pressure can be characterized in terms of both acoustic pressure and the convected, or hydrodynamic, pressure fluctuations. Prediction of the shell motion and sound radiated through the duct walls can only be made if an adequate space-time (alternatively, wavenumber-frequency) description of the wall pressure is known [1].

The long-term objectives of this research involve the measurement and study of sound generated by a ducted rotor system where the duct walls are constructed from thin, elastic, cylindrical shells. Specifically, a new facility has been created using a single 10 bladed propeller type rotor placed into a short cylindrical duct. The assembly was located in an anechoic environment that allowed for direct measurements of the radiated sound. The first component of this project involved the measurement and modeling of the rotor noise sources[2, 3]. The present paper describes results from the second phase of the project involving the description of the flow field and wall pressure in the region downstream of the rotor. Measurements involving the motion of the elastic duct and radiated sound will be considered in a future publication.

The wall pressure in the near-wake region of a rotor is extremely complex. The hydrodynamic pressure fluctuations result from blade wakes, tip-flow vortex motions, and the casing turbulent boundary layer. The blade wakes and tip flow features are particularly intense in the very near wake region, and decrease rapidly in the downstream direction. This results in pressure fluctuation levels and lengths scales that are strongly inhomogeneous in the streamwise direction. The flow also contains a mean swirl component resulting in a helical wake structure.

The nature of the acoustic field inside of a finite length duct is given by the characteristics of the noise source as well as the geometry of the duct. For the present experiments, the rotor can be considered to be the primary noise source. Sound is generated from the unsteady blade forces induced by turbulence in the approach flow, resulting in a dipole-like source. In general the spectral content of the blade noise can be characterized as a broadband component and a blade tone component. The tonal component of the sound results from the interaction of the rotor with mean

*Assistant Professor, Department of Aerospace and Mechanical Engineering, s.morris@nd.edu, AIAA Member
†Graduate Student, Department of Aerospace and Mechanical Engineering, David.B.Stephens.25@nd.edu, AIAA Student Member
‡ Undergraduate Student, Department of Aerospace and Mechanical Engineering, teconomo@nd.edu, AIAA Student Member
§Melchor Visiting Professor, Department of Aerospace and Mechanical Engineering, William.K.Blake.27@nd.edu, AIAA Member

inflow distortion as well as turbulence whose convected time scale is larger than the blade passing time. This results in multiple local maxima in the spectra at integer values of the blade passing frequency, or blade-rate (BR).

The sound field inside the duct is determined from the Green's function of a finite length duct that exhibits organ-pipe resonances, cross-flow radial modes, and spinning modes that cut-on at specific frequencies[4]. Subsequently, it will be shown that a significant source of the interior wall pressure, particularly at lower circumferential wavenumbers, is driven primarily by the interaction of these interior modes with the blade passing harmonics generated by the rotor.

The following section will describe the experimental facility and the measurement program. This will be followed by a detailed description of the streamwise development of the flow field in the wake of the rotor. The wall pressure will then be presented and interpreted in the context of the wake field data and the interior duct Green's function.

II. Experimental Program

Experiments were conducted in the ducted rotor assembly shown in Figure 1. The rotor was a 10 bladed propeller with a hub-to-tip ratio of 0.25, a diameter of 0.203m, and constant chord of 2.5cm. Each of the three duct sections located between the rotor and exit nozzle (grey sections in Figure 1) were interchangeable and machined to 0.203m in length and a diameter of 0.206m. The inlet region of the assembly spanned a length of 0.267m, while the entire assembly length from inlet to nozzle exit was 1.19m. A center-body was centered in the inlet section to support a servo motor. The propeller rotational speed could be specified up to 5000 RPM. The inflow conditions to the rotor were conditioned to minimize inlet disturbances. The primary source of noise was a result of the interaction between the rotor blades and the duct boundary layer. The region of interest for wall pressure measurements comprised the initial 0.203m of duct length immediately downstream of the rotor, which was contained within the first interchangeable duct section.

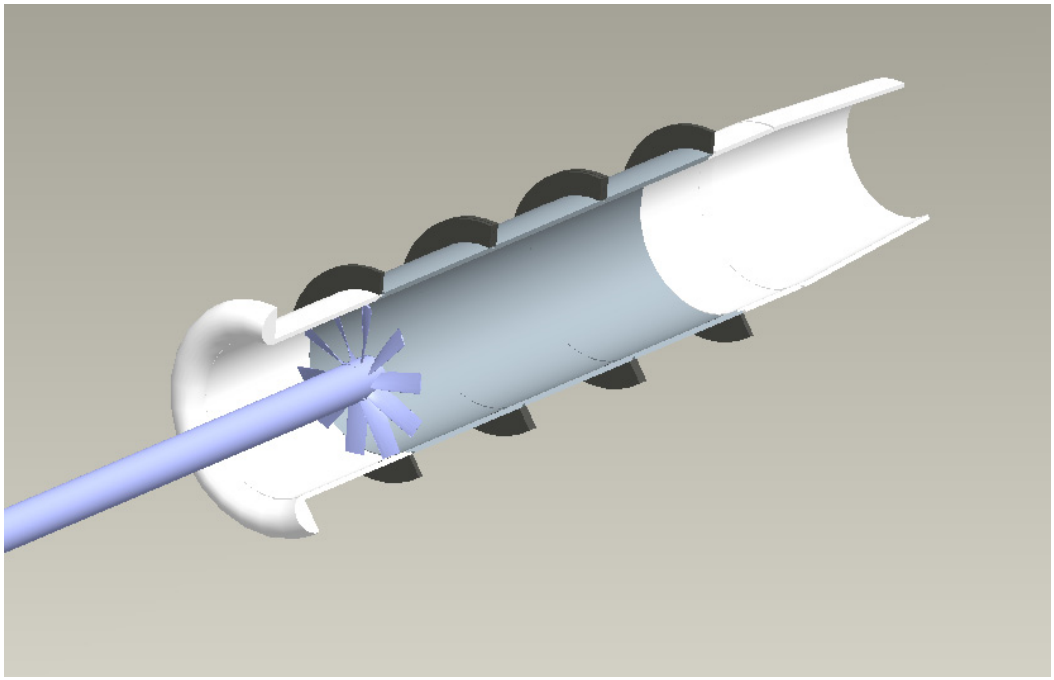

Figure 1. Schematic of the ducted rotor assembly.

The ducted rotor assembly was placed inside of two facilities within the Hessert Laboratory at the University of Notre Dame during two separate phases of data collection. First, the assembly was connected to a pressurized plenum. The duct sections downstream of the rotor were removed such that hot-wire surveys of the rotor exit flow could be obtained. The auxiliary blower connected to the plenum was set such that the net flow rate through the rotor/duct was identical to that which would have been obtained in the geometry shown in Figure 1. The flow field characteristics at multiple downstream locations were measured through hot-wire surveys. The measurements were acquired with a motor rotational speed of 4000 RPM. The axial locations of the surveys were 0.64cm, 3.18cm,

5.72cm, 10.80cm, 15.88cm, and 20.96cm downstream of the rotor. Each survey was completed using a radial and angular traverse mounted at the duct exit outside of the chamber. A laser trigger was sampled during the measurements to relate the velocity measurements to the rotational position of the blades. This allowed for a phase-averaged representation of the rotor wake, similar to what would be obtained by an observer moving in the reference frame of the rotor. The measurements were acquired using an X-wire probe that was calibrated before and after each traverse.

The second phase of the experimental measurements involved the measurement of the interior duct wall pressure. These measurements were conducted using only rigid duct sections downstream of the rotor. The assembly was placed within a large anechoic chamber with a low-end usable frequency limit of approximately 100Hz. The measurements utilized an array of 40 flush-mounted surface microphones. The sensing diameter of the microphones was 0.7mm. The array consisted of microphones distributed in both the circumferential and axial directions along one interchangeable duct section, as seen in Figure 2. Seven microphones spaced 1.9cm apart populated the axial row, and the upstream-most microphone was located 2.5cm behind the trailing edge of the rotor during data collection. The axial row shared one microphone with the circumferential ring of thirty-two evenly spaced microphones. The circumferential ring of microphones was located 10cm downstream from the trailing edge of the rotor. The array design was focused on the ability to gather meaningful measurements of the convecting flow field in two directions. Measurements were collected with the array duct section in the position directly downstream of the rotor. Each of the other two duct sections also contained one flush-mounted microphone for reference purposes. All microphone measurements passed through a 10Hz high-pass filter.

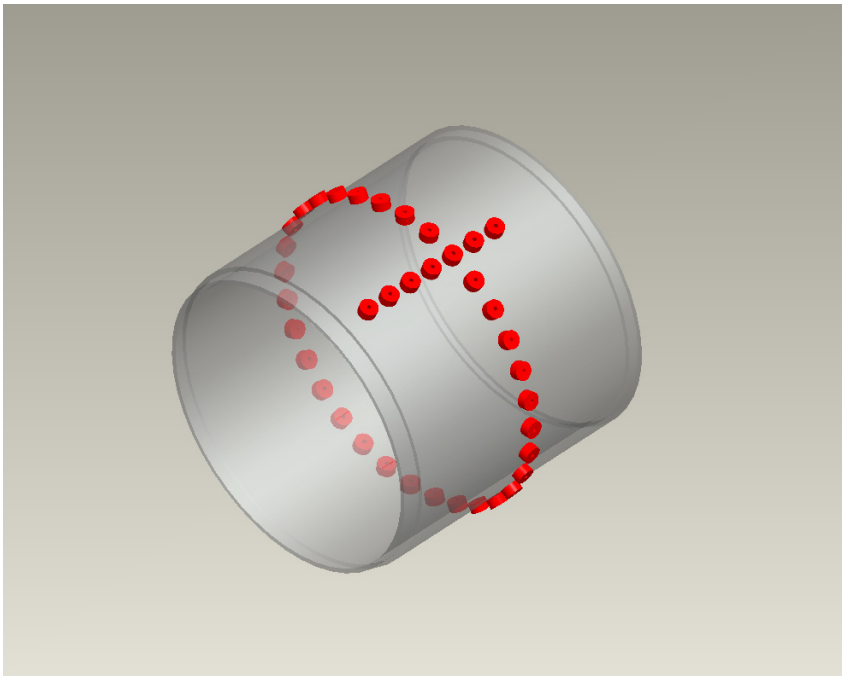

Figure 2. Flush-mounted surface microphones (red) in an interchangeable duct section.

The microphones were calibrated in situ in order to reduce movement of the apparatus between calibration and the experiment. All duct sections located downstream of the rotor were removed from the assembly intact and situated on a separate calibration stand. A speaker outputting white noise was positioned at the upstream end of the duct sections. Pressure data were collected from each of the microphones in the array as well as from a calibrated reference microphone positioned in the center of the duct. From the collected measurements, transfer functions were determined which calibrated the sound pressure spectral densities for each of the flush-mounted microphones to match that of the reference microphone over a large range of frequencies. The duct was assumed to contain only plane waves below the first cut-on frequency of 1000Hz.

III. Rotor Wake Measurement

The X-wire measurements at each downstream location were transformed into phase-averaged velocity profiles. The mean and RMS velocity inside the duct for the location 0.64cm downstream are presented in Figures 3 & 4. One readily visible characteristic of the flow field is the appearance of ten distinct blade wakes in both the mean and RMS profiles. The blade wake regions at this downstream location represent a decrease in the velocity to approximately 20% of the blade tip speed, down from a maximum near 30%. Further, the RMS velocity values rise to nearly 3% of the tip speed, or about 10% of the mean axial velocity in the duct.

A second characteristic is the casing boundary layer observable in both the mean and RMS profiles. The boundary layer thickness was approximately 10% of the duct radius. The effect of the blade tips on the boundary layer near the wall is apparent in the mean profile by the relatively low velocity regions near each of the ten blade tips. The RMS of the velocity was noted to be largest near the blade tips where the axial velocity was smallest. In these regions, the mean velocity drops below 15% of the blade tip speed and the RMS velocity reaches a maximum of near 7%, corresponding to nearly 22% intensity compared to the mean axial velocity in the duct.

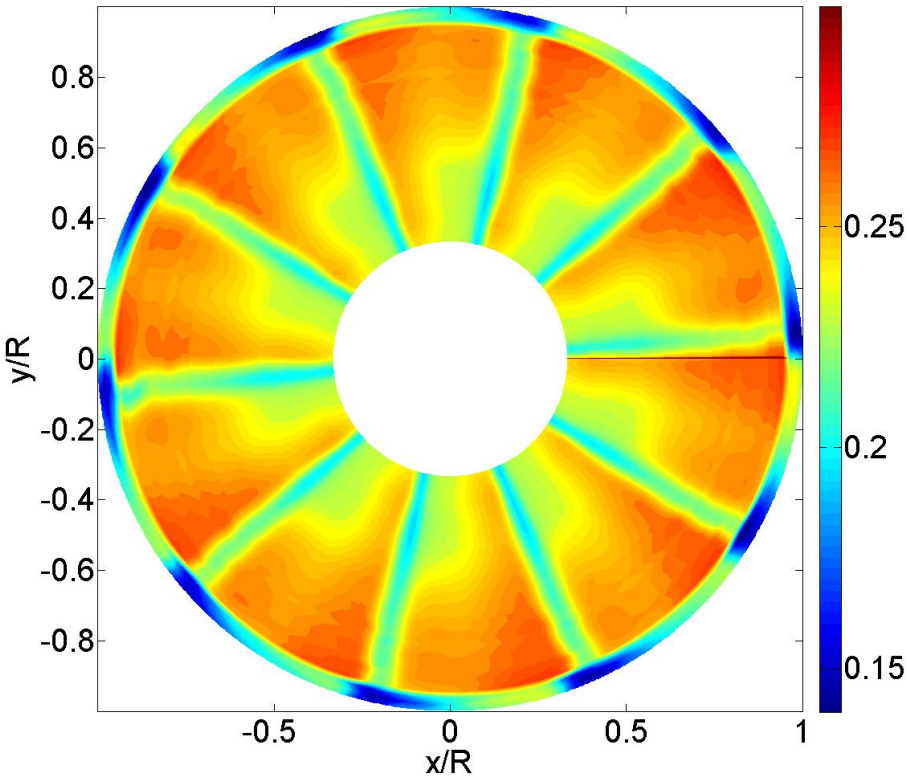

Figure 3. Mean phase-averaged velocity profile located 0.64cm downstream of the rotor. Velocities were normalized by the blade tip speed.

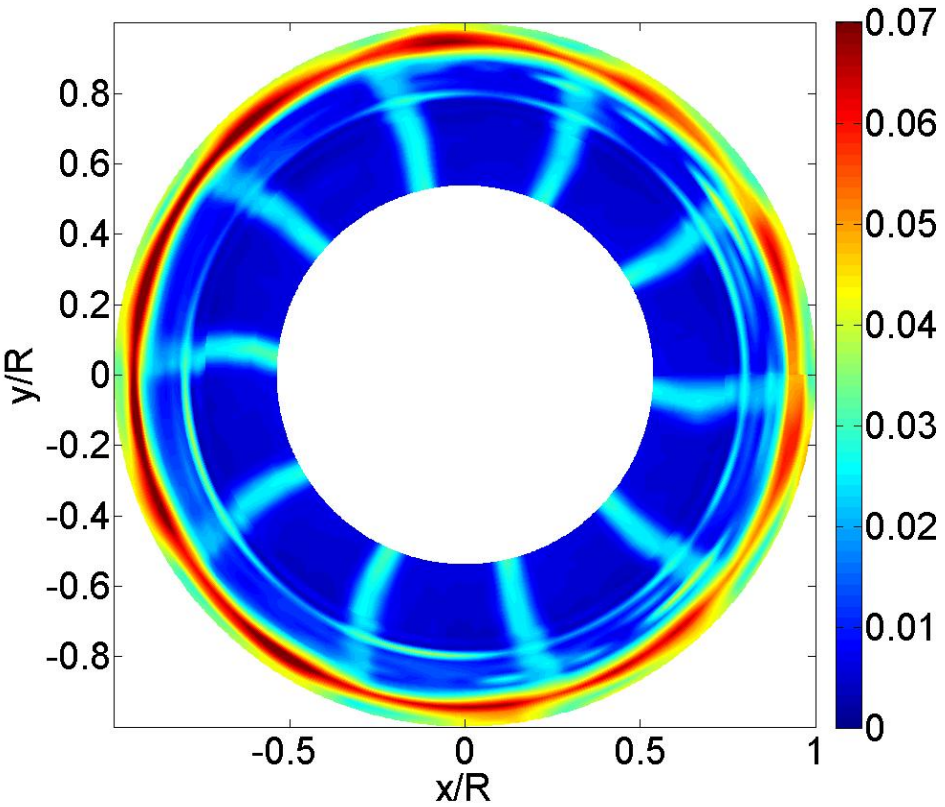

Figure 4. RMS phase-averaged velocity profile located 0.64cm downstream of the rotor. Velocities were normalized by the blade tip speed.

Multiple velocity surveys were conducted at various streamwise locations in order to document the development of the rotor wake. The phase-averaged velocity profiles for a single blade wake were plotted for locations at the beginning (0.64cm), middle (10.80cm), and end (20.96cm) of the region of interest. Profiles for two radii at these locations are presented in Figure 5. The first is at 86.8% of the maximum radius which lies in the mid-span of the blade outside of the boundary layer, while the second is at a radius of 95.7% which lies within the boundary layer near the wall.

At the mid-span radius, the velocity profiles exhibit distinct decreases in mean velocity within the blade wake region at all locations. The relative mean velocities remain constant around 25% of the tip speed, although each has a clear dip in magnitude representing the minimum mean velocity in the blade wake. Near the wall, however, the mean velocity profile does not exhibit this distinct decrease after the second downstream location, and even the profile of the second location has lost most of the shape from the first location downstream. The mean velocity magnitudes near the wall also do not vary considerably.

Of more value, however, is the evolution of the RMS velocity profiles at the three locations. Near the duct wall, the RMS profiles show little discernable pattern or correlation to the mid-span profile and remain at a magnitude near 12% of the tip speed. The mid-span profile at each location contains a significant peak in RMS magnitude in the blade wake. With an increase in downstream distance, the maximum RMS in the blade wake decreases from approximately 2.5% down to 1.5%. The decrease illustrates the rate of wake decay due to mixing.

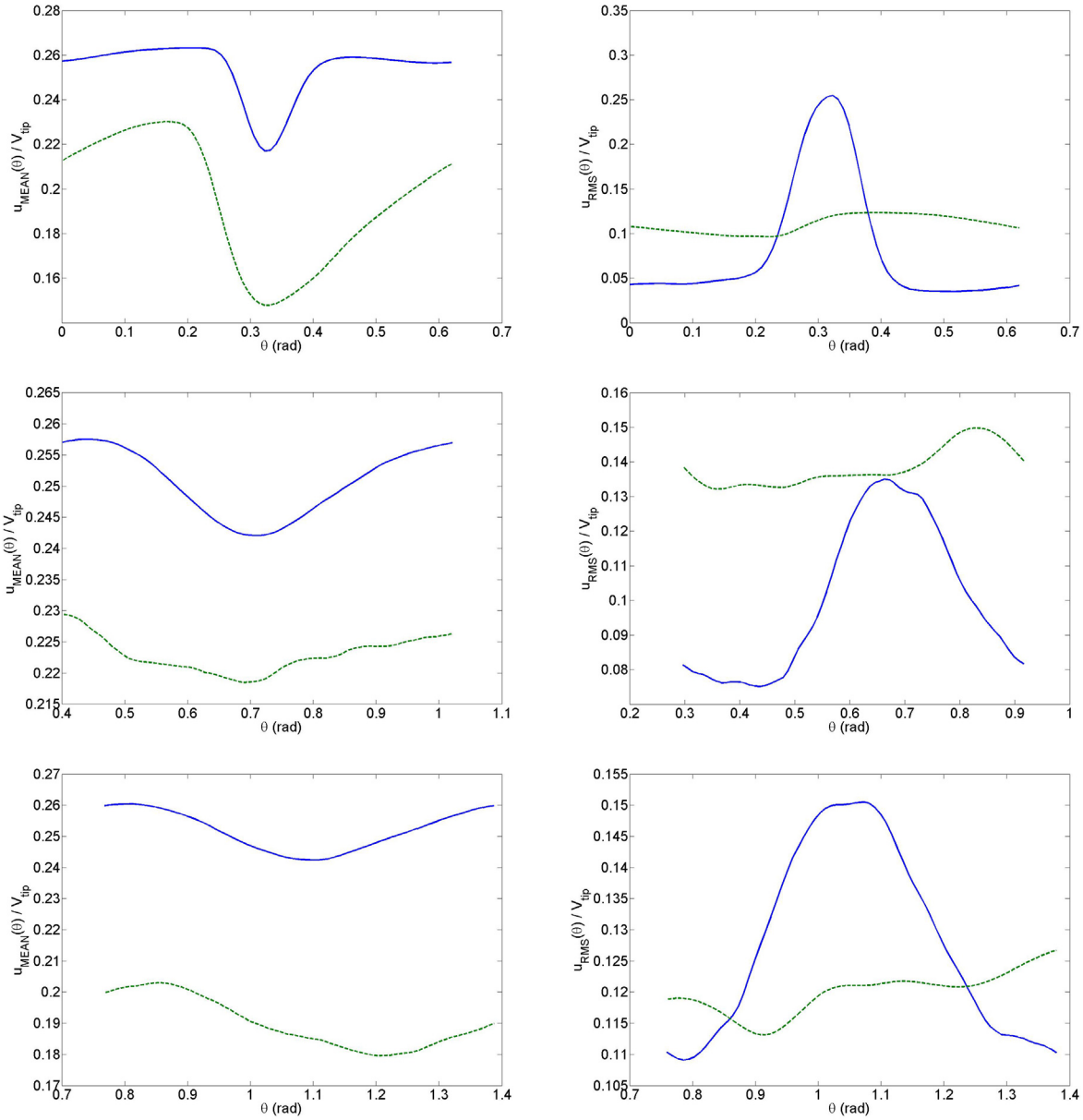

Figure 5. Mean (left column) and RMS (right column) velocity profiles of a blade wake at 0.64cm, 10.80cm, and 20.96cm downstream of the rotor (top to bottom). Values for a location near the tip (r/R = 0.957, dashed line) as well as for a mid-span location (r/R = 0.868, solid line) are presented. RMS values at the mid-span location have been multiplied by a factor of 10 for ease of viewing.

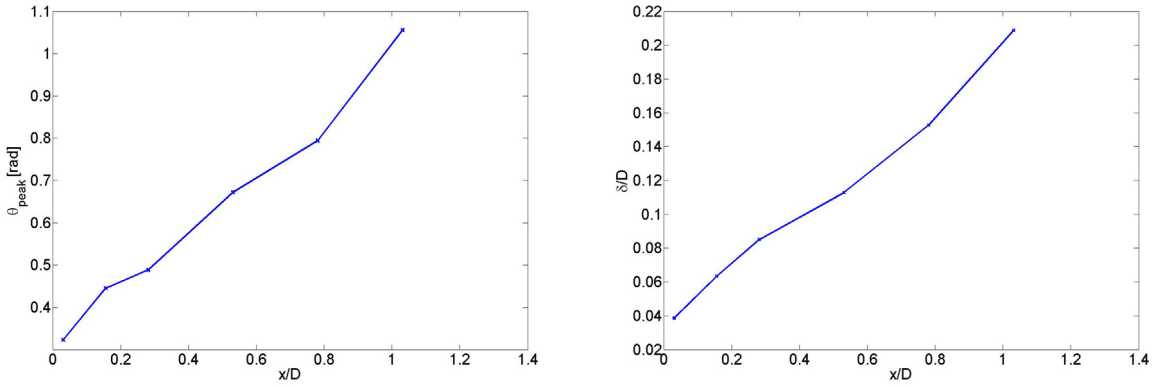

Figure 6. Phase location of the maximum RMS for the first blade wake observed at locations downstream of the rotor (left). Physical blade wake growth with axial distance downstream (right).

The mid-span RMS velocity profiles in Figure 5 also display important characteristics about both the swirl angle of the rotor wake as well as the growth of the blade wake thickness. The maximum RMS value of the blade wake at each location downstream occurs at a larger phase angle, signifying a swirling flow. For the three profiles in Figure 6, the maximum RMS values occur at approximately 0.3rad, 0.7rad, and 1.05rad. Figure 6 contains the location of the peak RMS values for each downstream survey, including those not presented in Figure 5. The trend is nearly linear, representing a relatively constant swirl rate. By the end of the region of interest, the flow has swirled from 0.3rad to 1.05rad, or a total of 0.75rad. Therefore, the rotor wake swirls approximately 12% of the circumference after traveling one diameter downstream.

The growth of the blade wake is apparent by the thickening of the peaks shown in the mid-span RMS profiles of Figure 5. The width of each peak was measured at 75% of its maximum RMS value for all downstream locations surveyed. Figure 6 contains the results normalized by the duct diameter. Immediately downstream of the rotor, the blade wake thickness is approximately 4% of the diameter. The thickness was observed to increase as a linear function of the streamwise distance.

IV. Wall Pressure Measurements

The wall pressure measurements were recorded at six speeds ranging from 2500 RPM to 5000 RPM. The RMS amplitude values from the axial microphone array are shown in Figure 7. The magnitudes were normalized by the tip speed, and show relatively good agreement. The decay in the RMS values with streamwise distance was significant, particularly in the first three microphone locations. This could be due to both a decay in the hydrodynamic pressures as well as a decay in the near-field acoustic pressures. Additional insight can be gained from the autospectral densities obtained at the various speeds. These are shown in Figures 8 & 9 for locations 2.5cm and 10cm downstream from the rotor, respectively. In order to aid in the presentation the spectral magnitudes from each speed were shifted by +10dB. Diagonal red lines were also inserted which correspond to the integer multiples of the blade passing frequency, and roughly line up with many of the local maxima in the spectra. In addition to the blade-rate related tones, a large number of spectral features can be observed, particularly at higher frequency. Many of these features can be correlated with the cut-on modes determined from the Green's function of a rigid cylindrical duct. These cut-on mode frequencies are labeled with the appropriate radial – circumferential mode number. These cut-on modes are observed to resonate at most speeds, but exhibit particularly strong resonant tones when the modal frequency and a multiple of the blade rate tone are in close proximity. This can be observed, for example, at 3000 RPM where the second harmonic of the blade rate corresponds to the first circumferential cut-on mode, resulting in a 10dB increase in the pressure at this frequency. In addition to the blade-tone cut-on mode interactions, the spectra exhibit significant complexity at higher frequency. This is particularly noticeable at the lower speeds. It appears that these are acoustic modes that are present at all speeds, but appear to be covered by the increasing broadband spectra.

The hydrodynamic and acoustic components of the pressure field can be roughly separated by considering how the blade rate amplitudes decay in the streamwise direction. Specifically, it is expected that the propagating acoustics will not be strongly dependent on the streamwise position, while the hydrodynamic contributions to the blade passing tones are expected to decay quickly. These results are shown for the lowest and highest speeds tested in Figure 10. At the lower speed, the amplitude of each blade-rate harmonic is observed to decay quickly in the

streamwise direction. The level observed at the most downstream measurement location was typically a factor of 10 lower compared with the location closest to the rotor. Note that the fourth blade-rate tone was observed to fall off more slowly, since the frequency coincides with the (0,2) acoustic mode of the duct.

At the higher rotor speed shown in Figure 10b, the decay in the streamwise direction was similar to the lower speed for the first blade-tone. However, the higher harmonics were less sensitive to the streamwise direction, and in some cases were nearly constant. This is most likely a result of the additional coincident frequencies between the blade-tones and the interior modes that exist at higher speed.

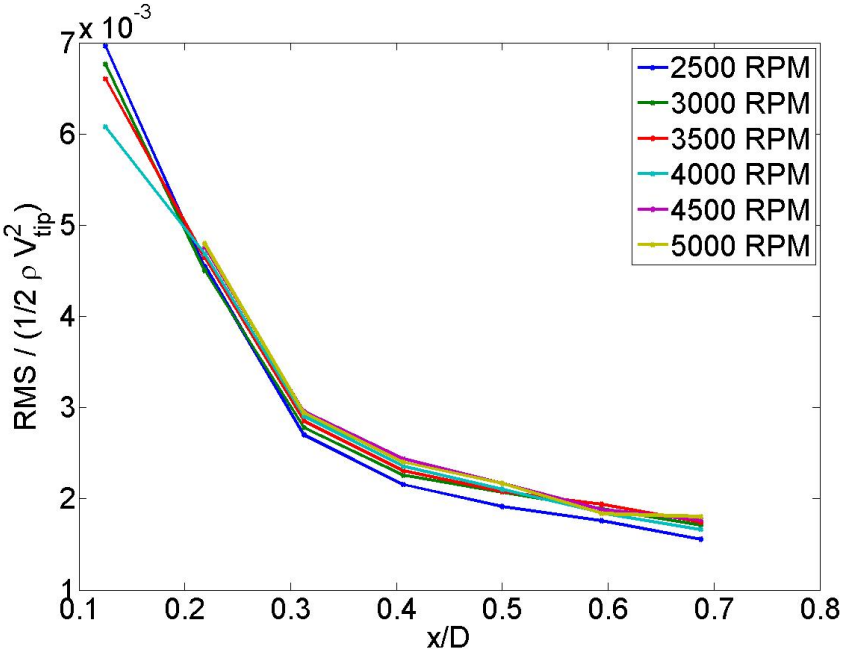

Figure 7. Mean RMS values of pressure measurements at each axial location for all rotor speeds.

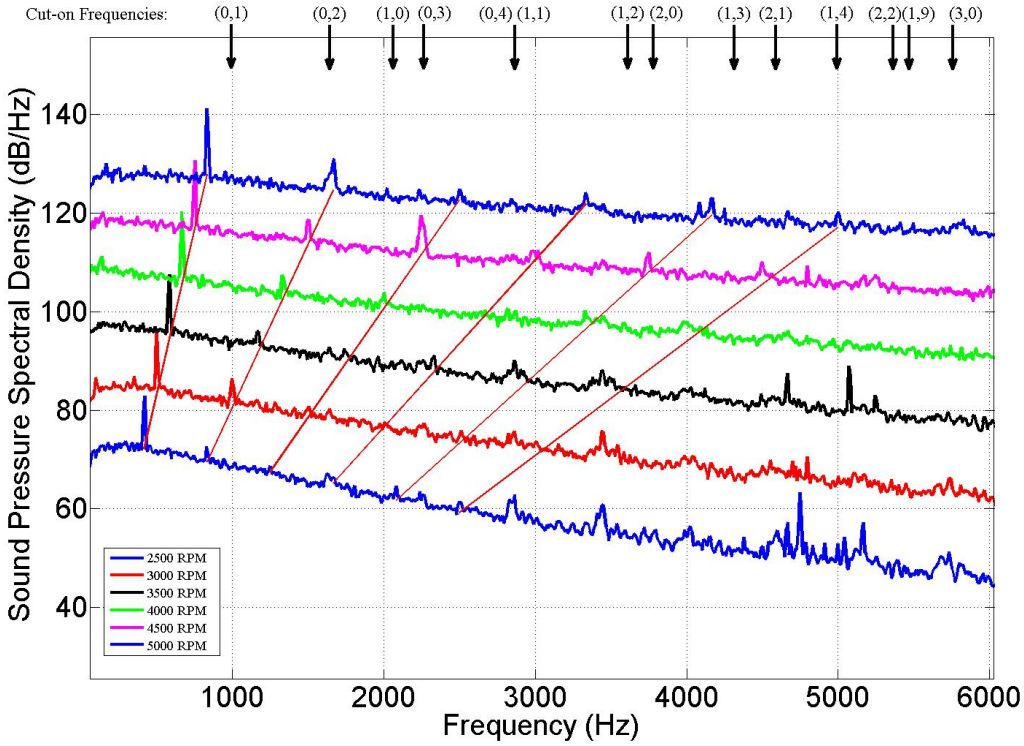

Figure 8. Autospectral density functions of wall pressure located 2.5cm downstream of the rotor at various speeds.

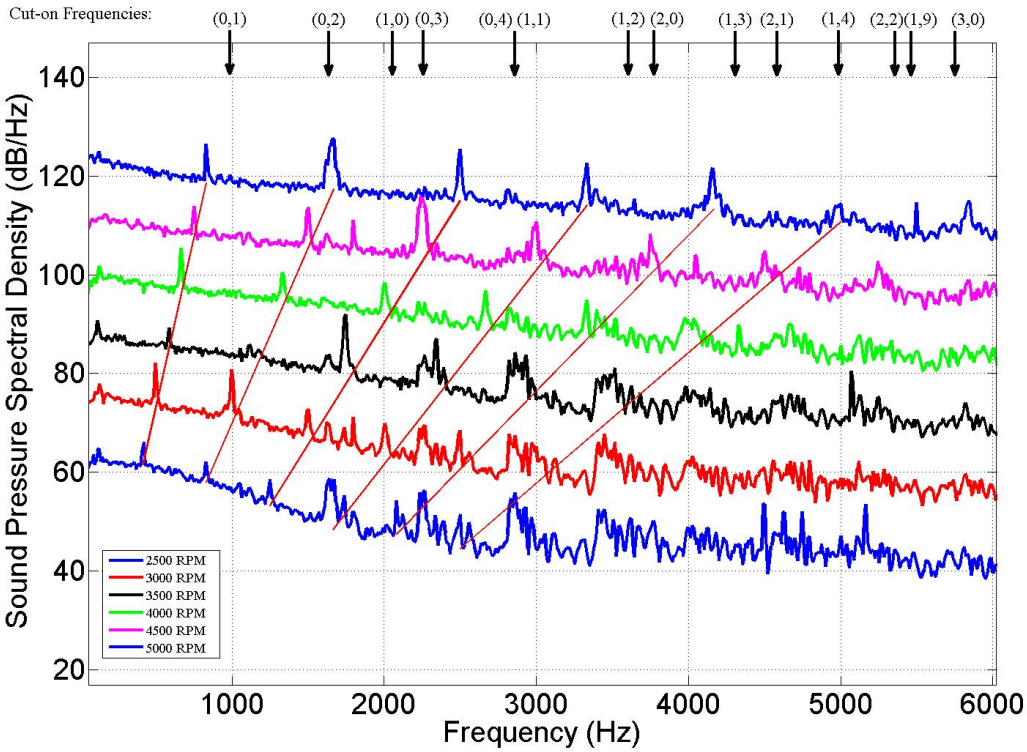

Figure 9. Autospectral density functions of wall pressure located 10cm downstream of the rotor at various speeds.

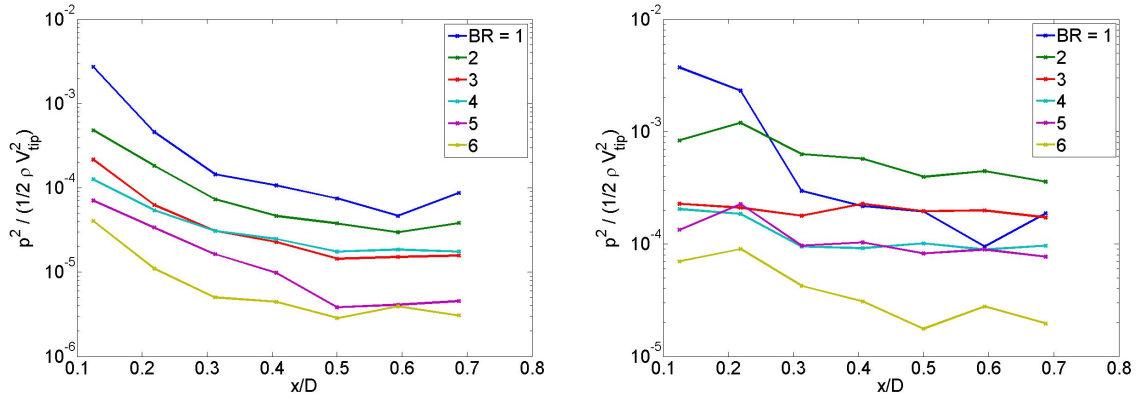

Figure 10. Wall pressure magnitude evaluated at multiples of the blade rate frequency at 2500 RPM (left), and 5000 RPM (right).

The final description of the interior duct wall pressure will make use of the circumferential array of 32 microphones as shown in Figure 2. The data were processed by applying the microphone calibrations and then computing the spatial Fourier transform of the cross spectral matrix values. These results are shown for 2500, 4500, and 5000 RPM in Figures 11, 12, and 13, respectively. The abscissa represents the circumferential mode order. The ordinate represents the frequency normalized by the blade rate frequency. A number of features can be observed that are common to the three rotor speeds shown. For the purposes of discussion the 2500 RPM case will be described first, and the differences noted at the higher speeds will then be commented on.

The modal-frequency contours shown in Figure 11 represent both the acoustic and hydrodynamic components of the flow field. At this speed the first cut-on mode (0,1) is at approximately 2.2 times the blade rate frequency. Thus, at ordinate values less than 2.2 only plane waves (n=0) can exist acoustically. The features that are readily observable as plane waves are the first and second harmonic of the organ pipe resonance (f /BR~0.25 and 0.5). Additional acoustic (n=0) fluctuations are observed at f /BR=1. At higher frequency. the acoustic modes are observable as a stepped 'V' shape in the contours. The steps represent the cut-on frequencies of the duct, where the left hand side (n<0) represents spinning modes in the direction of the rotor rotation, and n>0 represents modes spinning opposite of the rotor. As expected, the largest magnitudes are observed when the cut-on frequency corresponds to an integer value of f /BR. For example, the forth harmonic of the blade rate was observed to have a strong local maxima in Figure 8 at this rotor speed, and is clearly observed as the n=-2 mode in Figure 11. An additional feature of the acoustic modes observed within the duct are the multiple local maxima that are observed between the discrete steps of the cut-on frequencies. These features represent very high order harmonics of the axial (organ pipe) resonant frequency. Specifically, in a finite length duct the allowable axial wavenumber for higher order cross-stream modes are discrete, as opposed to the continuous spectrum of axial wavenumbers that are allowed for an infinite duct. Given the relatively large value of L/D=10 used for the present experiments, it was not anticipated that this would be a dominant feature of the higher order modes at very high frequency.

The hydrodynamic pressure fluctuations are not restricted to specific values of the circumferential wavenumber. Thus, all of the values observed outside of the 'V' shape are necessarily hydrodynamic. The magnitudes appear to be roughly constant with circumferential wavenumber, indicating the relatively small length scales of the turbulence in the duct boundary layer. The only observable feature is the local maxima noted at f /BR=1, n=-10 that represents the spinning blade wake pattern. The magnitude is observed to be roughly equal to the acoustic pressure at this frequency observed at n=0.

The modal-frequency contours observed at 4500 and 5000 RPM, shown in Figures 12 and 13, indicate a number of similarities with the lower speed case. However, the higher speed results in a much stronger interaction between the hydrodynamic field and the acoustic field because the dimensional blade passing harmonics are considerably stronger in the frequency range of the cut-on modes. For example, Figure 12 indicates a very strong interaction at f /BR=3, n=-3. Although this could be anticipated given the coincidence of the mode cut-on with the blade rate harmonic, large magnitudes are also observed in the hydrodynamic field (n<-3 and n>3) at this frequency. This suggests that the acoustic modes are also affecting the hydrodynamic pressure fluctuations. A similar observation can be made at the higher speed case shown in Figure 13. Specifically, the magnitude observed at f /BR=3 at higher circumferential order is reduced compared to the lower speed case. Additionally, the f /BR=2 is coincident with the (0,2) cut-on mode at this speed and is also observed to have large magnitudes at all n values.

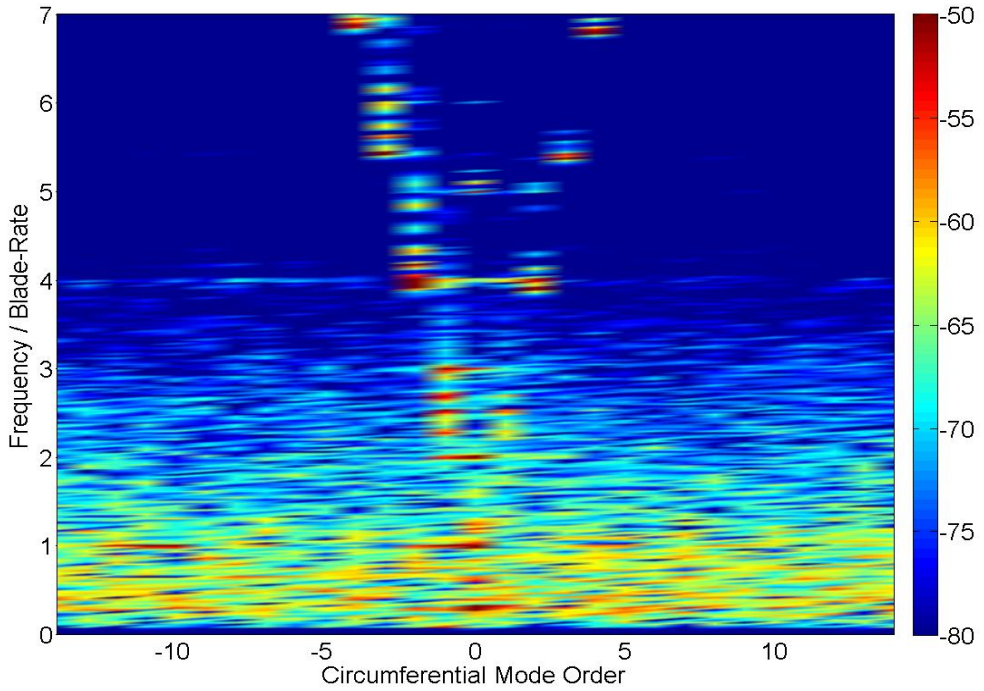

Figure 11. Pressure modes at 2500 RPM.

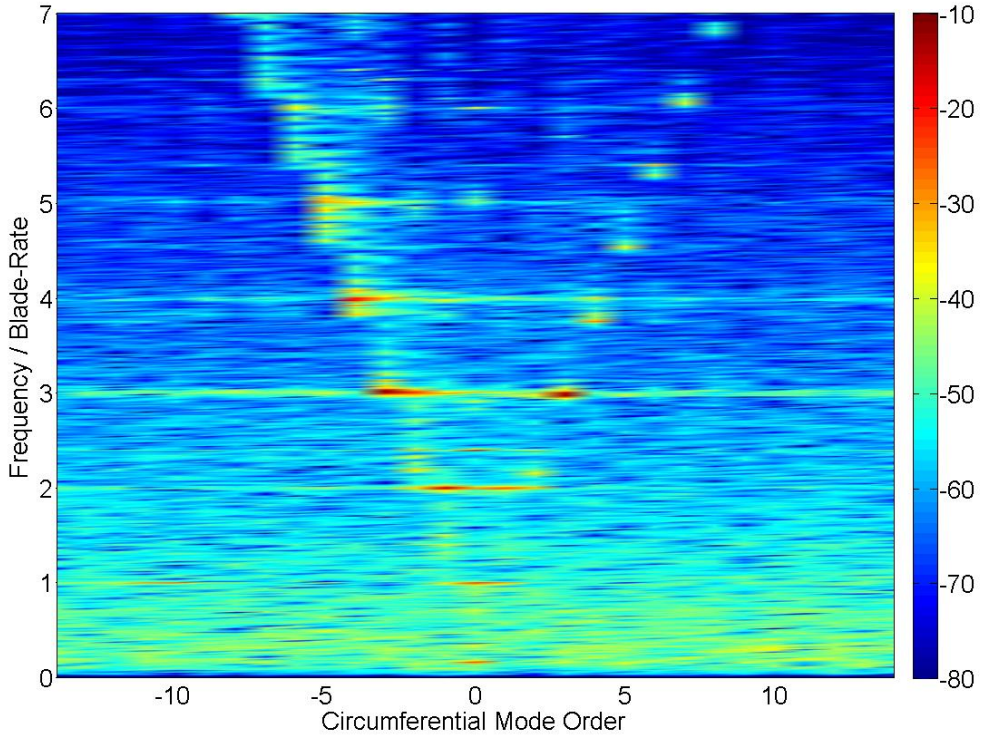

Figure 12. Pressure modes at 4500 RPM.

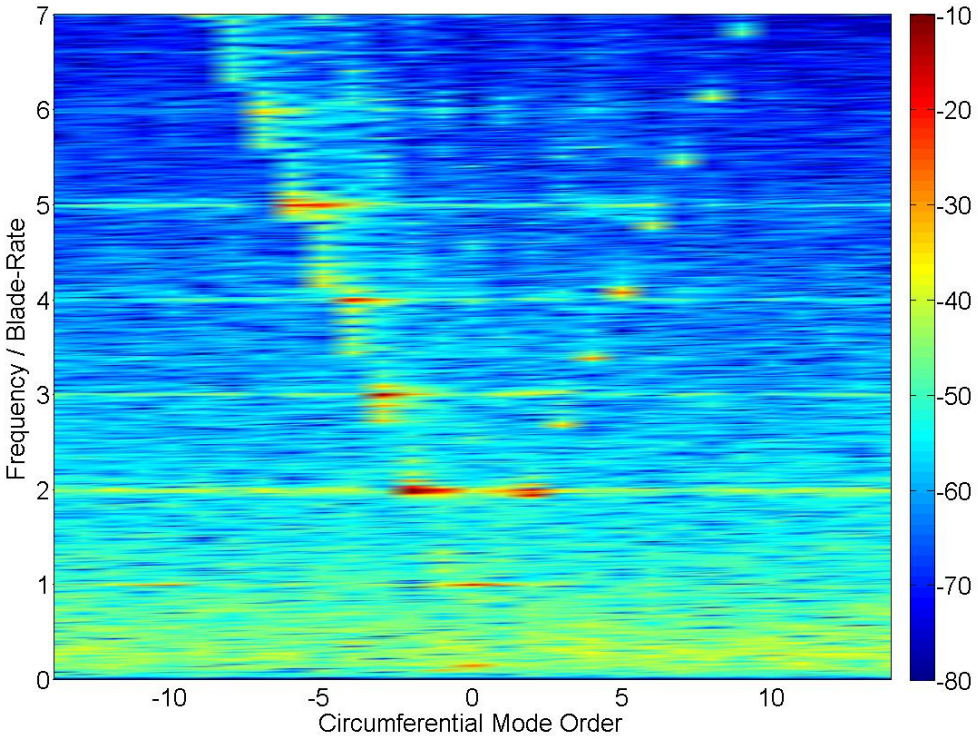

Figure 13. Pressure modes at 5000 RPM.

V. Conclusions

The data presented have been used to describe the velocity and pressure field characteristics in the near-wake of a ducted rotor. The velocity field indicated a pattern of swirling and decaying wakes, as well as a high level of turbulent fluctuations in the tip region. The wall pressure fluctuations resulting from these features were observed to decay rapidly in the streamwise direction. The acoustic pressures, as observed through the circumferential modal decomposition, indicated a strong interaction between the axial modes, the cross-stream cut-on modes, and the blade tones generated by the rotor. Future research will involve the use of the reported measurements to calculate the structural response of a thin elastic shell placed downstream of the rotor in the same experimental facility.

Acknowledgments

This research was made possible through funding from the US Office of Naval Research, Grant Number N00014-07-1-0570.

References

[1] Blake, W.K., *Mechanics of Flow-Induced Sound and Vibration,* Academic Press, Inc. 1986.

[2] Stephens, D.B. and Morris, S.C., 2008, "A method for quantifying the acoustic transfer function of a ducted rotor," J. Sound and Vib, 313, pp97-112.

[3] Stephens, D.B., Morris, S.C., and Blake, W.K., "Sound Generation by a Rotor Ingesting a Casing Turbulent Boundary Layer", AIAA 2008-2990

[4] Morse, P.M, and Ingard, K.U., *Theoretical Acoustics*, Princeton University Press, 1968.